Renewable Energy 239 (2025) 121921

Contents lists available at ScienceDirect

Renewable Energy

journal homepage: www.elsevier.com/locate/renene

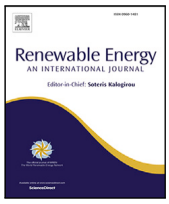

Power and thrust control by passive pitch for tidal turbines

Stefano Gambuzza [a], Puja Sunil [a], Mario Felli [b], Anna M. Young [c], Riccardo Broglia [b], Edward D. McCarthy [d], Ignazio Maria Viola [a,*]

[a] School of Engineering, Institute for Energy Systems, University of Edinburgh, Robert Stevenson Road, Edinburgh, EH9 3FB, Scotland, United Kingdom
[b] Institute of Marine Engineering (INM), National Research Council (CNR), Via di Vallerano 139, Rome, 00128, Italy
[c] Department of Mechanical Engineering, University of Bath, Bath, BA2 7AY, England, United Kingdom
[d] School of Engineering, Institute for Materials and Processes, University of Edinburgh, Robert Stevenson Road, Edinburgh, EH9 3FB, Scotland, United Kingdom

ARTICLE INFO

Keywords:
Renewable energy
Tidal turbine
Passive pitch system
Power and thrust control
Unsteady load mitigation

ABSTRACT

Tidal turbines operate in unsteady and non-uniform flows and thus experience large load fluctuations. In this study, we explore the effects of changes in freestream velocity and yaw misalignments on the performance of a turbine equipped with passively pitching blades. We compare the experimental results from a 1.2-m-diameter turbine in a recirculating open channel facility and numerical results based on blade-element-momentum theory. The thrust remains approximately constant with increasing free stream speed, meaning that the structural load on the turbine is minimised. While not held constant, the power increases at less than half of the rate of a turbine with fixed pitch blades. This finding shows that power can be controlled effectively by changing the tip speed ratio, allowing, for example, the power to be capped at a rated value by marginally increasing the angular velocity. Furthermore, the power and thrust are found to be negligibly sensitive to yawed incoming flow compared to a fixed-pitch turbine. Overall, these results demonstrate that passive pitch is a viable alternative to active pitch, and pave the way for further development of this technology.

1. Introduction

Tidal energy is a predictable and reliable renewable energy source that can greatly contribute to energy security [1]. The slow variations of the tidal flow velocity over the timescale of a day are highly predictable because they depend predominately on the relative position of celestial bodies and on the geography of the tidal site [2]. Tides can be described through the superimposition of waves, of which the most significant is the semi-diurnal lunar constituents with a period of 12.421 h. At the most energetic tidal sites such as, for example, the Pentland Firth, flow velocity switches from more than $5\,m\,s^{-1}$ in one direction to the same amount in the opposite direction twice a day [3]. The wide range of operating conditions means that turbines typically adopt an active collective pitch control system [4], where all blades pitch simultaneously. Active pitch systems of this kind ensure that the turbine can self-start when the flow speed is slow, cap the maximum power to protect the generator when the flow speed is high, and stop the turbine in case of emergency.

Tidal turbines also experience large variations in inflow speed and direction over shorter time scales than can be mitigated with collective pitch control [5,6]. Unsteadiness in the flow may arise due to wave-induced current [7], yaw, shear and turbulence [8]. The mean flow speed of a tidal stream varies with depth, resulting in a vertically sheared flow profile such that the blade experiences a variable load depending on its polar position. Turbulence intensities are as high as 20%, correlated to vortical structures with scales of tens of metres generated at the seabed [9]. In addition, there may be variations in blade loading due to blockage, interaction with neighbouring turbines [10,11], tower passing perturbations, angular velocity fluctuations, and flow-induced structural vibrations. In contrast to the wind energy sector, blockage due to side-by-side arrangement of the turbines is desirable because it increases the energy flux through the rotor-swept area [12–14]. Model scale measurements [11] have demonstrated that constructive interference can enable up to a 20% uplift in power.

Earlier studies have characterised the effect of flow unsteadiness on the blade root bending moment, thrust and torque of tidal turbines through experiments and numerical simulations. For example, experiments conducted in a towing tank [15,16] show phenomena consistent with delayed separation and dynamic stall for blade rotations at low tip speed ratio. These effects result in a significant increase in the root bending moment that exceeds the steady load by up to 25% with significant hysteresis, while tests in a wave tank indicate a maximum load range of 100% and 175% of the in-plane and out-of-plane bending moments, respectively [17].

* Corresponding author.
E-mail address: i.m.viola@ed.ac.uk (I.M. Viola).

https://doi.org/10.1016/j.renene.2024.121921
Received 15 April 2024; Received in revised form 6 November 2024; Accepted 14 November 2024
Available online 26 November 2024

Nomenclature

a	Axial induction factor
a'	Tangential induction factor
c	Sectional blade chord [m]
C_d	Sectional drag coefficient
C_l	Sectional lift coefficient
C_m	Sectional moment coefficient about the quarter-chord point
C_P	Power coefficient
C_T	Thrust coefficient
D	Rotor diameter [m]
d	Sectional drag [N m^{-1}]
f	Blade thickness [m]
f_ψ	Sectional force along the polar direction [N m^{-1}]
f_X	Sectional force along the streamwise direction [N m^{-1}]
f_x	Sectional force along the chordwise direction [N m^{-1}]
f_y	Sectional force along the chord-normal direction [N m^{-1}]
k	Spring constant [N m rad^{-1}]
l	Sectional lift [N m^{-1}]
m	Sectional moment about the quarter-chord point [N m^{-1}]
M_P	Moment on one blade about the pitching axis [N m]
m_P	Sectional moment about the pitching axis [N m^{-1}]
M_s	Elastic moment of the torsional spring [N m]
N	Number of samples
P	Power generated by the turbine [W]
P_{rated}	Maximum power at rated flow speed [W]
P_{ref}	Power at reference conditions [W]
Q	Torque on the rotor about the turbine axis [N m]
Q_b	Torque on one blade about the turbine axis [N m]
r	Radial coordinate [m]
r_{hub}	Hub radius [m]
r_{tip}	Radial coordinate of the blade tip [m]
Re	Reynolds number
Re_c	Chord-based Reynolds number
T	Thrust on the rotor [N]
t	Time [s]
T_{ref}	Thrust on the rotor at reference conditions [N]
T_b	Thrust on one blade [N]
u_{rated}	Rated flow speed [m s^{-1}]
u_∞	Freestream flow speed [m s^{-1}]
w	Weighting factor
X	Streamwise coordinate [m]
x	Chordwise coordinate [m]
x_{tr}	Chordwise coordinate of the laminar-to-turbulent transition point [m]
x_P	Chordwise coordinate of the pitching axis [m]
y	Chordnormal coordinate [m]
y_P	Chordnormal coordinate of the pitching axis [m]
$\boldsymbol{e}_\psi$	Unit vector in the polar direction
$\boldsymbol{e}_X$	Unit vector in the streamwise direction
$\boldsymbol{W}$	Inflow flow velocity vector [m s^{-1}]
α	Angle of attack [°]
β	Pitch angle [°]
β_{pre}	Spring preload angle [°]
γ	Yaw angle [°]
λ	Tip-speed ratio
λ_{rated}	Optimum tip-speed ratio at rated flow speed
ν	Kinematic viscosity [m^2 s^{-1}]
ω	Angular velocity [rev min^{-1}]
ω_{rated}	Optimum angular velocity at rated flow speed [rev min^{-1}]
ψ	Polar coordinate [m]
ρ	Fluid density [kg m^{-3}]
σ	Standard deviation
τ	Tidal period [s]
θ	Twist angle [°]

Several active control systems for unsteady load reduction have been developed for wind turbine rotors [18], such as trailing edge flaps [19–21], leading edge slats [22,23], and microtabs [24,25]. Trailing-edge flaps can decrease fatigue loads by 5% to 15% for most components of wind turbine blades [26]. Actively controlled flaps and trips have also been tested on a model-scale tidal turbine [27] and shown to alleviate fluctuations in thrust and torque, respectively. Individual pitch control, where every blade can pitch independently by the other blades, can decrease load peaks by 30% on both rotating and non-rotating components [18]. However, the need for complex engineering systems such as blade pitch control systems, and gearboxes can increase the operational costs, need for frequent maintenance and potential for failure [24]. Additionally, seabed-mounted turbines require a minimum of three cable cores to connect to the shore for controlling the active pitch system, and the reliability of these cores is a significant challenge [28].

Recently, there has been an increased focus on developing passive control systems for unsteady load mitigation. Passive control can be achieved either by modifying the blade camber or by introducing changes in the blade twist, known as aeroelastic tailoring or passive adaptive blades. The blade camber can be changed, for example, by deploying a flap, which attenuates blade vibrations and increases fatigue life [29]. Arredondo-Galeana et al. [30] showed theoretically and experimentally that the load alleviation of trailing edge flaps is proportional to the ratio of the flap length to the chord length.

Adaptive camber airfoils were demonstrated to reduce fluctuating loads by up to 60% while generating more mean lift than a rigid reference airfoil [31]. Bio-inspired hyperflexible turbine blades can reduce flow separation and stall. A reduction in the structural loads by 25% and in the blade thrust by 20% compared to an equivalent rigid blade was demonstrated experimentally [32].

Passive adaptive blades with bend-twist coupling are designed to smooth load fluctuations by twisting towards feather when a gust causes increased loading, and away from feather when the loading drops [33]. Model-scale experiments showed up to 11% lower peak thrust loads and a 15% reduction in peak power compared to a turbine with rigid blades. Passive adaptive blades can be combined either with overspeed control or active pitch control [34]. Experiments have shown that the passive adaptive blade combined with overspeed control

can produce constant torque with minimum thrust increments. While the blade twist dominates thrust changes, flapwise blade deformations have a significant impact on the power performance [35], and can be exploited for power capping above the rated flow speed.

Unsteady load alleviation can be achieved by a foil through passively pitching in response to onset flow changes. The foil can be kept at a mean angle of attack by a torsional spring or by applying a constant external torque. Numerical simulations showed that an optimum choice of the pitching axis could result in a reduction of the lift fluctuations of more than 80% [36]. A mathematical framework for the identification of the pivot point location that maximises unsteady load mitigation was developed by Otomo et al. [37]. The concept of a passive pitching foil was first explored by Viola et al. [38], who conceptualised the use of a passive pitch system on a turbine to maintain either constant thrust or torque. The first theoretical model was proposed by Pisetta et al. [39]. The authors showed that the thrust fluctuations can be mitigated by passively and elastically adjusting the pitch, resulting in no change to the mean torque and, thus, to the harvested power. This model was investigated numerically by Dai et al. [40], who performed a CFD analysis on a turbine with blades that were each attached to the hub by a torsional spring, allowing each blade to pitch passively about its axis. The rotor operated through a shear layer and the passive pitch showed a lower amplitude thrust and torque fluctuation than a fixed pitch blade. Experimental tests were performed by Gambuzza et al. [41] on a 1.2 m-diameter turbine in the FloWave Ocean Energy Research Facility, a 30-m-diameter 2-m-deep recirculating open channel. The blades were connected to the hub through a torsional spring. The torque and thrust fluctuations due to turbulence and shear were significantly mitigated by the passive pitch. The spring stiffness and preload were chosen to match the hydrodynamic time-averaged pitching moment, such that the time-averaged pitch angle was the same as the pitch angle of an equivalent fixed-pitch blade.

The above-mentioned studies demonstrated the mitigation of fluctuations due to shear and turbulence. These fluctuations have a period of the order of seconds. The passive pitch system investigated in these earlier studies could be used, for example, together with an active system that varies the pitch over the tidal period. However, the slow changes in flow velocity happening over a tidal cycle correspond to low-frequency fluctuations happening over hours. Turbines typically adopt an active pitch system that adjusts the rotational speed to maintain rated power when the flow speed exceeds a threshold.

The present study focuses on the ability of the passive pitch system to replace an active pitch system, viz. to mitigate fluctuations within a period of the order of hours, such as due to changes in the mean flow speed over the tidal period. Therefore, the present tests are performed in a low turbulence facility with a uniform onset flow without shear. Furthermore, this experimental setup allows complementing previous studies on the mitigation of high-frequency fluctuations by considering load variations due to yaw misalignment with a uniform flow stream.

Specifically, this study aims to address the following questions. (1) How would a turbine equipped with a passive pitch system perform at different flow speeds when the angular velocity is adjusted to keep the optimum tip speed ratio? (2) What is the effect on thrust and power of a change in the angular velocity? (3) Can this effect be exploited to further control the loads on the turbine beyond the passive pitch by actively adjusting the angular velocity and, for example, to maintain rated power when the flow speed exceeds a threshold? Therefore, can a passive pitch system entirely replace an active pitch control system? (4) How would such a system behave when the turbine is misaligned with the free stream by a yaw angle? (5) finally, can the performances of the turbine equipped with a passive pitch system be accurately predicted with a low-order model such as, for example, blade element momentum theory?

The rest of the paper is organised as follows. In Section 2, we describe the experimental facility, the turbine, and the low-order model based on Blade Element Momentum Theory that we used to design the passive pitch system. In Section 3, we describe the design of the passive pitch system. Here, passive pitch is achieved by means of a torsional spring that allows the blades to pitch along an axis parallel to the spanwise axis of the turbine. The optimal position of the pitching axis with respect to the blade is discussed in this section (Section 3). In Section 4, we present the results of the experimental campaign with the model scale tidal turbine, where the effect of freestream velocity, tip speed ratio, and yaw angle on the thrust and torque is investigated. Finally, in Section 5, we use the experimental results to analyse the performance of a hypothetical turbine equipped with passively pitching blades over a tidal cycle and compare the energy yield with that of a turbine equipped with state-of-the-art active pitch control.

2. Methodology

2.1. Facility

The experimental campaign was carried out in the recirculating open water channel at the Institute for Marine Engineering of the Italian National Research Council (CNR-INM), in Rome, Italy. The facility is often used for model-scale tests of propellers and ships (see, for instance, [42,43]), and has a test section with a rectangular cross-section of size $3.6\times2.25\ \mathrm{m}^2$ and a useable length of 10 m; previous studies have found a turbulence intensity of 4% and negligible shear [42,44]. The water temperature is measured by an immersed thermocouple; this measurement is then used to estimate the water density ρ and kinematic viscosity ν according to the relations presented by [45,46], respectively.

2.2. Turbine and pitching system

The turbine used in this experimental campaign is a speed-controlled, three-bladed turbine with a rotor diameter $D = 1.2\,\mathrm{m}$. The turbine shaft is connected to that of a DC machine, which is an in-house system to allow testing of rotor systems at CNR-INM. The system allows pitch and yaw rotations and vertical displacements of the turbine.

The turbine hub was submerged at a depth of $0.8\,\mathrm{m} = 0.67D$ from the free surface, and the blade tips were submerged by $0.2\,\mathrm{m} = 0.17D$ at their uppermost position. The turbine was tested with freestream speeds u_∞ of between $0.4\,\mathrm{m\,s^{-1}}$ and $0.7\,\mathrm{m\,s^{-1}}$; resulting in a range of diameter-based Reynolds number, $Re \equiv u_\infty D/\nu$, from 2.4×10^6 to 4.2×10^6.

The main components of the turbine are outlined in Fig. 1, where we also define the main reference frame used during this work. This is a cylindrical reference frame rotating with the turbine, having as its axis the turbine rotor axis: distances along this direction are represented by the coordinate X, with its origin on the rotor-swept plane; the radial coordinate is denoted with r and the polar coordinate (out-of-plane in Fig. 1) is labelled ψ. As the blades used here are free to pitch, the rotor-swept plane is defined as the plane swept by the pitching axes during the turbine rotation; in this reference frame, the pitching axis of the first blade is the straight line at $X = 0, \psi = 0$, while the axes of the other two blades are at $\psi = 2\pi/3$ and $\psi = 4\pi/3$ respectively. Each turbine blade (A) is mounted on the pitching system (B), (see Fig. 2 for detail), and the pitching system is attached to the turbine hub (C). The hub is, in turn, directly mounted on a bespoke load transducer. The signals from the transducer are then routed through the slip-ring assembly (E), to a cable connected to a data acquisition board. Further details of the acquisition chain and the data reduction stage are given in Section 2.3.

The passive pitching apparatus is shown in Fig. 2 in exploded view, to give a clear view of all the components. The turbine blade (A) is mounted on a spacing arm (B), which sets the distance between the blade and the pitching axis (E); by changing the mounting arm it is possible to change the position of the blade with respect to the pitching axis, and thus the performance of the system. The rotation of the pitching axis (and, therefore, of the blade) is constrained by two components: the torsional spring (C) and a retention and limiting

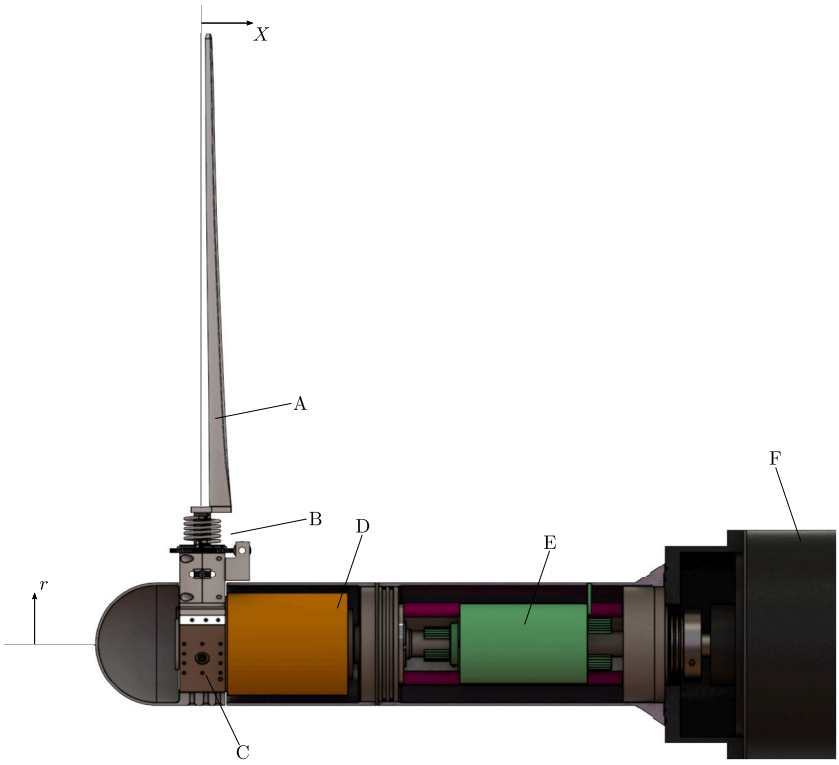

Fig. 1. Sketch of the turbine used during this experimental campaign with annotated components: (A) turbine blade; (B) passive pitching system; (C) turbine hub; (D) load cell and transducer; (E) slip ring assembly; (F) brushless DC generator. Fairings are shown in sectioned view for clarity.

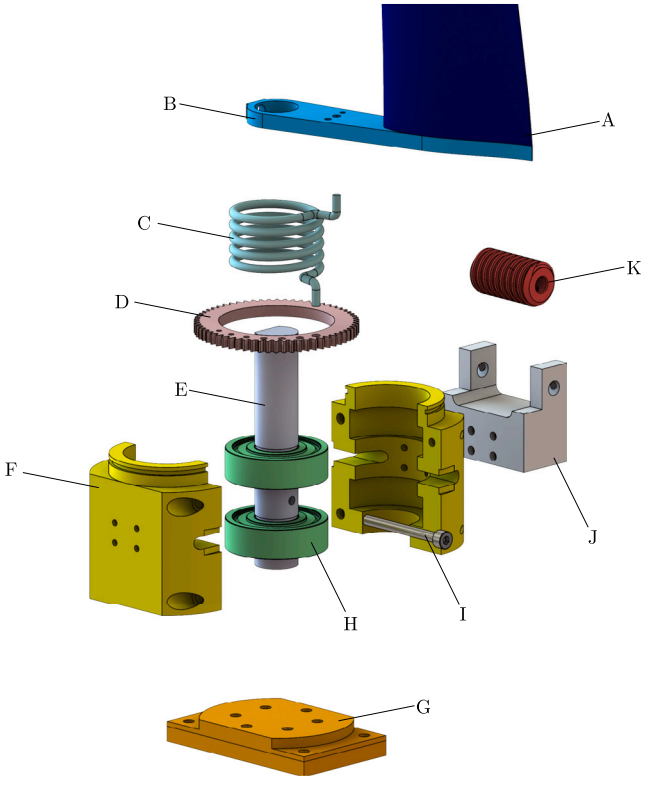

Fig. 2. Exploded view of the passive pitching mechanism, with annotated components: (A) turbine blade; (B) spacing arm; (C) torsion spring; (D) preload spur gear; (E) pitching shaft; (F) mechanism frame; (G) mounting plates; (H) ball bearings; (I) retention and limiting screw; (J) preload worm mounting frame; (K) preload worm.

screw (I). The torsional spring is manufactured so that its legs extend axially: these engage at the top end with a hole in the mounting arm, and at the bottom end with holes on the top face of a spur gear (D); this gear, in turn, engages with a worm (K), which locks the rotation of the spur gear. The worm is mounted on the frame (J) by means of a bolt (not pictured), to which it is secured. The bolt is turned manually by means of a key: this turns the worm and consequently the spur gear and the bottom leg of the spring, thus setting the preload of this system. The shaft (E) is constrained by the retention and limiting screw, which is engaged on a threaded hole on the shaft: as the shaft rotates, the screw moves in a slot cut in the two frame halves (F), constraining the shaft rotation to a range of 25° in each direction. Alternatively, the screw can be fastened until the screw head engages on a flat surface cut on the frame halves: under this configuration, the shaft is prevented from rotating and the system behaves as a fixed-pitch blade. The torsional spring used during these tests is manufactured from a spring steel wire with diameter 2.05 mm; the spring has 5 coils and a external diameter of 40 mm, and has a winding height of 24 mm. The estimated spring constant for this geometry and Young's modulus of 200 GPa is $\kappa = 0.276\,\mathrm{N\,m\,rad^{-1}}$. The torque can be accurately modelled as constant because its variations are small within the operational range. In fact, the torque generated by the spring varies linearly with the angular position of the blade, β. This varies by less than 8° within the operational condition range, as discussed in Section 4.1. The spring preload is $\beta_{\mathrm{pre}} = 447.5°$, and thus the torque variations are estimated in less than 1%.

The turbine blade geometry is reported in Table 1: this reports, for a number of radial stations along the blade at a distance r from the turbine axis, the local chord c, the local twist θ (measured as the angle between the local chord and the rotor-swept plane, positive if the leading edge is upwind), the local thickness f and the position of the section quarter-chord point relative to the pitching axis of the turbine x_P and y_P. These last quantities are measured as the schematic in Fig. 3: x_P is the distance along a direction parallel to the section chord between the section quarter-chord Q and the pitching axis P, while y_P

Table 1
Blade table, reporting the radial position of each section r, the local chord c, twist θ, and thickness f, along with the position of the quarter-chord of each section relative to the pitching axis x_P and y_P.

r/D	c/D	θ [°]	f/c	x_P/c	y_P/c
0.115	0.112	17.62	0.24	−1.00	0.11
0.125	0.112	15.66	0.24	−1.00	0.08
0.150	0.111	12.35	0.23	−1.00	0.03
0.175	0.108	10.87	0.23	−1.00	0.01
0.200	0.105	9.96	0.22	−1.00	0
0.250	0.099	8.91	0.20	−1.00	0
0.300	0.093	8.00	0.19	−1.00	0
0.350	0.088	7.03	0.17	−1.00	0
0.400	0.086	6.21	0.16	−1.00	0
0.450	0.083	5.74	0.14	−1.00	0
0.495	0.073	5.50	0.13	−1.00	0

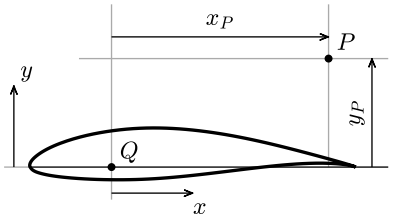

Fig. 3. Definition of the section-based reference frame, along with x_P and y_P for a blade section (defined positive as in the figure): Q is the quarter-chord of the particular section and P is the intersection between the pitching axis and the section plane.

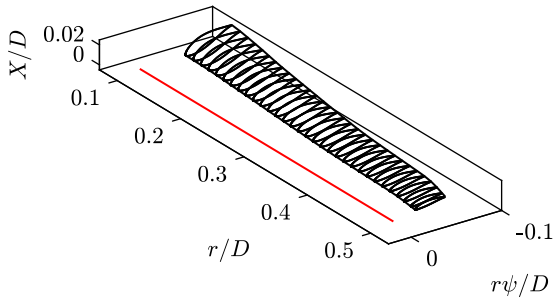

Fig. 4. Three-dimensional representation of the blade sections (in black) and their position relative to the pitching axis (in red.

is similarly measured in a direction perpendicular to the local chord; x_P is positive if the pitching axis is behind the quarter-chord (going towards the foil trailing edge), and y_P is positive if the pitching axis is above the chord (going towards the suction side of the foil). As x_P is negative for all blade sections, the blade pitches around an axis located ahead of the blade. Note that Fig. 3 also defines a reference frame in the section plane, whose coordinates are denoted by lowercase letters: in this, x represents the coordinate along the chordwise direction, positive from the trailing to the leading edge, and y represents the chord-normal coordinate, positive from the pressure to the suction side. This coordinate system has its origin on the quarter-chord of each section, and moves with the section as it pitches. All sections of the turbine blade are aerofoils belonging to the NACA 63-8XX family, where the last two digits are, in hundredths, the thickness-to-chord ratio f/c. The blade geometry is shown in Fig. 4, in which a selection of the blade sections has been plotted, along with the location of the pitching axis with respect to the blade in solid red; a full 3D model of the blade is available in the dataset associated with this publication.

2.3. Acquisition chain and data reduction

The data acquired in this experimental campaign consists in the thrust T and torque Q generated by the turbine at different values of either freestream speed u_∞ or turbine tip-speed ratio $\lambda \equiv \omega r_{\text{tip}}/u_\infty$, where ω is the turbine angular velocity and $r_{\text{tip}} = D/2$. All data is available on the Edinburgh DataShare at the hyperlink https://doi.org/10.7488/ds/7842.

Data are acquired by a force and torque transducer (component (D) in Fig. 1) mounted on the DC machine shaft, to which the turbine rotor is bolted on; thus, the measured loads are those generated by all three blades, with no information on the loading of each individual blade. When these loads are presented as functions of the tip-speed ratio, they are reported as the thrust C_T and power coefficient C_P, which are defined as $C_T \equiv 2T/(\rho u_\infty^2 \pi r_{\text{tip}}^2)$, and $C_P \equiv 2Q\omega/(\rho u_\infty^3 \pi r_{\text{tip}}^2)$, (with the mechanical power generated by the turbine estimated as $P = Q\omega$). The force and torque transducer is a bespoke load cell manufactured by Applied Measurements: this is rated for a maximum load of 1300 N in the axial direction and a maximum torque of 100 N m about the same axis; the maximum loads generated by the turbine during this experimental campaign have been a thrust of 145 N and a torque of 11.5 N m, well below the transducer limits. Calibration of the transducer has been carried out by the manufacturer, and no further efforts to calibrate it have been carried out; the relationship between the load cell current output and the acquired forces is linear.

The load measurements were acquired from the load cell by taking the difference in the output of the load cell under load and its mean output under no load, (i.e., the zero reading, which was taken at least once per day with the facility stopped and no flow circulating in the test section). The load cell output consists of two 4 mA to 20 mA signals that were transferred, via the slip-ring, to a data acquisition board (a National Instruments cDAQ system with a NI-9203 analogue input card). Data were acquired at a frequency of 500 Hz for a duration of 60 s for the load cell zero readings and 300 s for the force and torque measurements under load.

2.4. Blade element-momentum theory

As will be seen in Section 3, knowledge of the expected inflow conditions and of the blade performance is necessary to prescribe the correct distribution of pitching axis coordinates, x_P and y_P, along the blade. As is customary in wind and tidal energy applications, this design work was carried out using a low-order code implementing Blade Element-Momentum Theory (BEMT). In the case of this work, the software suite transTide [7,8] was used to estimate the flow around the turbine blade under operation; transTide implements the approach of [47] to solve the BEMT equations and find the induction factor.

While the transTide code used here allows for estimating the performance of the blade under a turbulent, sheared inflow, this functionality was disabled for the results here presented, and the flow around the turbine blade was instead estimated for laminar, uniform inflow only. The stopping criteria of the BEMT is such that the relative difference between the induction factors computed at the last and second last iterations is lower than 10^{-5}. The BEMT equations are solved with the inclusion of Glauert's root- and tip-loss correction factors [48]. For high axial induction factors, the empirical formula of Buhl [49] is used to approximate the real behaviour of the turbine at high induction factors. The solution of the BEMT equations is computed on 100 equally spaced sections along the turbine blade. Time-advancement of the solution is carried out by assuming a constant induction factor. It is assumed here that the lift and drag coefficients vary quasi-steadily with the angle of attack α and no effect of the angle of attack history is seen on the aerodynamic coefficients. The simulations are run for five full rotations of the rotor.

This code takes as inputs the polar curves of each section of the blade, which were computed via XFOIL [50]. Two polars were computed for each section of the blade: a low-Reynolds-number polar is obtained by imposing $\lambda = \lambda_1 = 4$ and a forced transition of the boundary layer

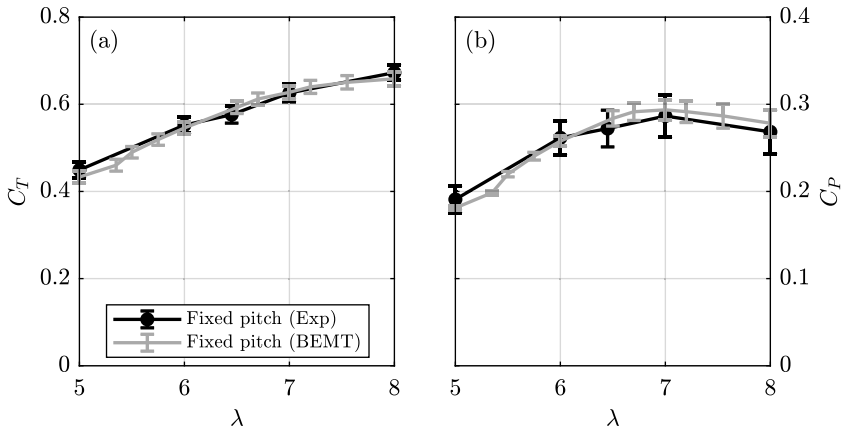

Fig. 5. Thrust (a) and power (b) versus tip-speed ratio as measured experimentally and estimated from the BEMT code. Error bars show the 95% confidence interval of the experimental measurements and BEMT simulations.

at $x_{tr}/c = 2/3$ on both sides of the hydrofoil, while a high-Reynolds-number polar imposes $\lambda = \lambda_2 = 8$ and $x_{tr}/c = 1/4$. The chord-based Reynolds number for each section was computed as

$$Re_c \equiv \frac{u_\infty \sqrt{1 + \left(\frac{\lambda r}{r_{tip}}\right)^2}\, c}{\nu}, \tag{1}$$

where $u_\infty = 0.5\,\mathrm{m\,s^{-1}}$. The lift coefficient of any section at a given tip-speed ratio λ was obtained by a weighed sum of the two computed polars: defining $C_l^{(1)}$ to be the lift coefficient computed at $\lambda = 4$ and $C_l^{(2)}$ to be that at $\lambda = 8$, the final C_l is found as

$$C_l = (1 - w)\, C_l^{(1)} + w\, C_l^{(2)}, \tag{2}$$

where

$$w = \begin{cases} 0 & \lambda < \lambda_1 \\ \frac{1}{2}\left(1 - \cos\left(\pi \frac{\lambda - \lambda_1}{\lambda_2 - \lambda_1}\right)\right) & \lambda_1 < \lambda < \lambda_2 \\ 1 & \lambda_2 < \lambda \end{cases}. \tag{3}$$

The same procedure was repeated for the drag and quarter-chord moment coefficients C_d and C_m.

Fig. 5 shows the thrust and power coefficients C_T and C_P of the turbine used in this work, both measured in the facility and estimated from the BEMT code. The data shows that there is good agreement between the experimental data and the predictions for all values of λ. The maximum difference in C_T between experiments and BEMT is nearly 3% at $\lambda = 5$, while the uncertainty in C_P is nearly 3.5% at $\lambda = 8$. The 95% confidence interval is shown with error bars in Fig. 5. The uncertainty of the experimentally measured thrust and power coefficients is computed, assuming a normal distribution, as $2\sigma/\sqrt{N}$, where σ is the standard deviation and N is the number of samples. Because this formulation is strictly valid only for independent samples, σ and N are computed for a time history resampled at a frequency u_∞/D. The uncertainty in the BEMT simulations is based the method of Liu et al. (2024). Monte Carlo simulations are performed using a normal distribution of lift and drag coefficients with a standard deviation equal to three times the difference between the coefficients computed with Xfoil and CFD for 2D blade sections. The uncertainty on the BEMT estimates of thrust and power is about 6% in C_P and 2.7% in C_T at $\lambda = 8$.

3. Passive pitch system design

The purpose of this section is that of offering a mathematical framework with which to estimate the optimal position of the blade with respect to the pitching axis. Referring to the schematic of Fig. 3, this means finding a distribution of $P(r) = (x_P(r), y_P(r))$ to guarantee that a certain performance is achieved. The purpose of this section is to give a mathematical framework for the estimation of the optimal position of the pitching axis for a given performance requirement, i.e., finding the distribution of $P(r) = (x_P(r), y_P(r))$. For instance, one might distribute the sections to ensure that the thrust transferred from each blade to the turbine structure be constant before and after a change in freestream speed. To achieve this aim, we will introduce an algorithm to estimate the performance of a pitching blade after a change in the inflow conditions, having fixed $P(r)$; as this is computationally inexpensive, a suitable $P(r)$ can be found by iterating over this algorithm via exhaustive search.

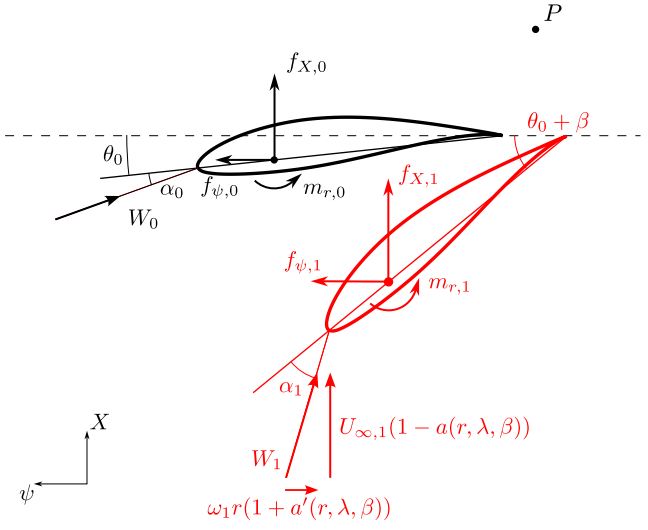

Fig. 6. Schematic diagram of a blade section undergoing pitching, before (in black) and after (in red) a change in the observed freestream velocity from $\boldsymbol{W}_0$ to $\boldsymbol{W}_1$. The dashed line shows a direction parallel to the rotor-swept plane.

Fig. 6 is a schematic of the forces and moments generated by a blade section undergoing a pitching motion as a result of a change in blade loading; in this diagram, the subscript 0 refers to the steady state conditions before the change, and the subscript 1 refers to those after the change. Note that the cause of the change in blade loading is not specified. For example, it could due to a change in the freestream speed u_∞ during a tidal cycle, a change in the turbine yaw or in its angular velocity ω, or due to the blade section rotating through a sheared inflow. As a result of the loading change, the blade pitches by an angle β: this value is a function of the loads on the blade before and after the

change in inflow, as well as the position of each section of the blade with respect to the pitching axis, which is the design consideration.

To estimate the loading and position of the blade before and after the change, one can follow the BEMT approach outlined in Section 2.4. In this, the total inflow velocity $\boldsymbol{W}$ seen by a section is

$$\boldsymbol{W} = u_\infty(1 - a(r,\lambda,\beta))\,\boldsymbol{e}_X + \omega\, r(1 + a'(r,\lambda,\beta))\,\boldsymbol{e}_\psi\,, \tag{4}$$

where a and a' are the axial and tangential induction factors, respectively, $\boldsymbol{e}_X$ and $\boldsymbol{e}_\psi$ are the unit vectors in the axial and polar directions, and β is the uniform pitch angle of the blade, which is initially zero. The induction factors are a function of the position along the blade span r, the tip-speed ratio λ, and the blade pitch β. Each section of the turbine blade generates a moment m around an axis perpendicular to it, and two forces applied on the quarter-chord point. These can for instance be expressed as the lift l and drag d, with the drag being parallel to the local velocity $\boldsymbol{W}$ and the lift perpendicular to it; their magnitudes are

$$l(r) = \frac{1}{2}\rho\, W^2(r)\, c(r)\, C_l(\alpha, r)\,, \tag{5}$$

$$d(r) = \frac{1}{2}\rho\, W^2(r)\, c(r)\, C_d(\alpha, r)\,, \tag{6}$$

$$m(r) = \frac{1}{2}\rho\, W^2(r)\, c^2(r)\, C_m(\alpha, r)\,, \tag{7}$$

where ρ is the fluid density, $W = |\mathbf{W}|$, c is the blade chord at a given span, and C_l, C_d, and C_m are the lift, drag, and moment coefficients of each section, as a function of the angle of attack α seen by each section. Note that these forces and moments are per unit span and are denoted by lowercase letters. Alternatively, one can consider the projection of the forces onto the turbine reference frame, as shown in Fig. 6, for which

$$\begin{bmatrix} f_X \\ f_\psi \end{bmatrix} = \begin{bmatrix} \cos(\alpha+\theta) & \sin(\alpha+\theta) \\ \sin(\alpha+\theta) & -\cos(\alpha+\theta) \end{bmatrix} \begin{bmatrix} l \\ d \end{bmatrix}. \tag{8}$$

With these, the total thrust T_b and torque about the turbine axis Q_b generated by each blade can be expressed as

$$T_b = \int_{r_{\text{hub}}}^{r_{\text{tip}}} f_X \,\mathrm{d}r\,, \tag{9}$$

$$Q_b = \int_{r_{\text{hub}}}^{r_{\text{tip}}} r\, f_\psi \,\mathrm{d}r\,, \tag{10}$$

where r_{hub} is the radial coordinate of the blade section closest to the turbine axis. The mathematical notation for this framework is made simpler by choosing to express the forces in the section reference plane defined in Fig. 3:

$$\begin{bmatrix} f_x \\ f_y \end{bmatrix} = \begin{bmatrix} -\sin(\alpha) & \cos(\alpha) \\ \cos(\alpha) & \sin(\alpha) \end{bmatrix} \begin{bmatrix} l \\ d \end{bmatrix}. \tag{11}$$

These forces can be estimated with knowledge of the induction coefficients a and a', which can be obtained, for each tuple (r,λ,β), from a BEMT solver such as the one outlined in Section 2.4. Note that these solutions only require knowledge of the blade geometry and the aerodynamic properties of each blade section: no knowledge of the position of each section with respect to the pitching axis is necessary, and these steps can be carried out prior to any consideration on $P(r)$. Therefore, knowing the solution of the BEMT problem for a range of tip-speed ratios and blade pitch angles, one knows the forces and moments generated by each section of the blade

$$f_x = f_x(r,\lambda,\beta,u_\infty)\,, \tag{12}$$

$$f_y = f_y(r,\lambda,\beta,u_\infty)\,, \tag{13}$$

$$m = m(r,\lambda,\beta,u_\infty)\,. \tag{14}$$

These contribute to the moment per unit span about the blade pitching axis, which can be expressed as

$$m_P(r) = f_x\, y_P - f_y\, x_P + m\,, \tag{15}$$

Table 2
Changes in inflow and operating conditions.

	u_∞ [m s^{-1}]	ω [rad/s]	λ
Before	0.5	5.375	6.45
After	0.7	5.375	4.61

while the blade as a whole generates a total pitching moment

$$M_P(\lambda,\beta,u_\infty) = \int_{r_{\text{hub}}}^{r_{\text{tip}}} m_P \,\mathrm{d}r = \int_{r_{\text{hub}}}^{r_{\text{tip}}} (f_x\, y_P - f_y\, x_P + m)\,\mathrm{d}r\,. \tag{16}$$

In addition to this, the blade sees an elastic moment applied by the torsional spring which can be assumed to be a linear function of pitch angle β

$$M_s(\beta) = \kappa\,(\beta + \beta_{\text{pre}}) \tag{17}$$

where β_{pre} is the preload of the spring, which is set so that at the initial steady-state the elastic moment balances the blade pitching moment

$$M_s(0) = \kappa\,\beta_{\text{pre}} = M_P(\lambda_0,\beta_0,u_{\infty,0})\,, \tag{18}$$

where $\beta_0 = 0$. To simplify the calculations, one can assume that the spring elastic moment be constant, instead of linearly varying with β, which is a reasonable assumption if $\beta_{\text{pre}} \gg \beta$. The experimental results presented in Section 4 have been obtained with a spring preloaded by $\beta_{\text{pre}} = 447.5°$, while the value of β is limited by the pitch mechanism to $\pm 25°$, and so this assumption is reasonable. Labelling λ_1 the turbine tip-speed ratio after the change in inflow conditions, the final geometric pitch of the blade can be obtained as the value of $\beta = \beta_1$ for which the total pitching moment is equal to the initial one

$$M_P(\lambda_1,\beta_1,u_{\infty,1}) = M_P(\lambda_0,\beta_0,u_{\infty,0})\,, \tag{19}$$

which can be solved numerically to yield β_1 and, once this is known, the total forces generated by the blade can be found, and thus the performance of the turbine after the change in inflow conditions. Computationally, this framework requires knowledge of both the BEMT solution over a suitable subspace of (λ,β), and a one-dimensional root-finding algorithm to determine the performance of the blade given a particular choice of $P(r)$. In particular, as the solution of the BEMT problem does not depend on $P(r)$, in order to estimate the performance of the blade after a change in inflow for different distributions of $P(r)$, one only needs to solve Eq. (19) for each proposed $P(r)$. As this only requires numerical integration and a one-dimensional root-finding algorithm, it is computationally inexpensive, and the optimal position of the blade with respect to the pitching axis can be found, for instance, by exhaustive search.

For this work, we are interested in the particular case for which the turbine presented in Table 1 undergoes a change in the freestream speed u_∞ during the tidal cycle, while keeping its angular velocity constant. In particular, for this, we impose the operating conditions before and after the change in inflow as specified in Table 2. In this work, the distributions of $P(r)$ have been constrained such that x_P/c and y_P/c are constant along the blade span. This simplifies the BEMT analysis, but is not strictly necessary, as one could have computed the final position of the blade after a change in the inflow velocity based on the equilibrium of the total moments acting on the three-dimensional blade.

Fig. 7 shows the values of thrust and power generated by the turbine after the change in inflow conditions, normalised by the loading before the gust, as a function of $P(r)$. It can be seen in the figures that the values of thrust and torque after the change in operating conditions are only minimally affected by the actual position of the blade with respect to its pitching axis, especially if the axis is located upstream of the blade leading edge ($x_P = -0.25$, $y_P = 0$). In fact, it can be seen that there is a large region, that for which $x_P/c < 0$, where the thrust and power after the gust are insensitive to the actual values of $P(r)$. The largest change in T_1 and P_1 with the pitching axis position is

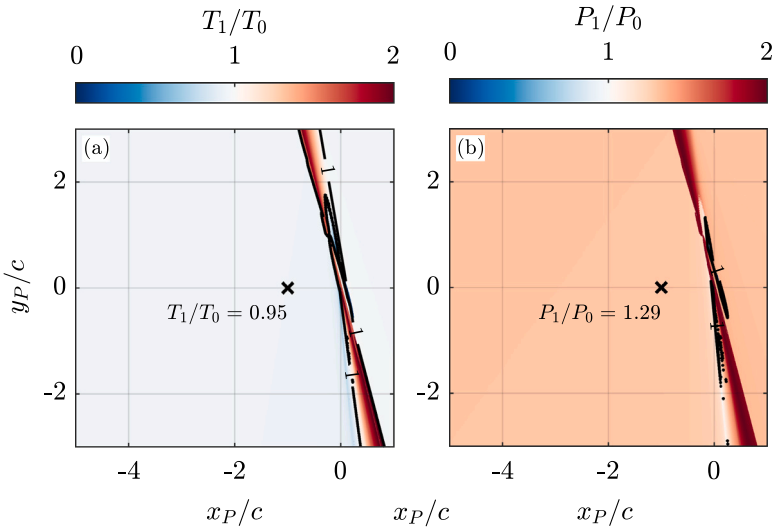

Fig. 7. Thrust (a) and power (b) after a change in operating conditions according to Table 2 with a change in the position of the blade with respect to the pitching axis.

concentrated in a narrow band roughly above and below the turbine blade; in particular, there is a clear locus of points for which the thrust after the inflow change is equal to that before the change. While a turbine designer might therefore choose to place the blade sections so that $T_1/T_0 = 1$ or $P_1/P_0 = 1$, one must note the high sensitivity of the turbine loads after the gust to the pitching axis location near the lines for which the load ratio is 1. In fact, any wrongful estimation of the inputs to the mathematical framework here described will move these loci significantly; such an error might come for instance from a mis-estimation of the lift, drag, or moment coefficients of the individual blade sections; from non-linearity of the spring used to counteract the pitching moment seen by the blade; from manufacturing tolerances in the construction or assembling of the turbine; or from a change in inflow conditions which does not mirror that under which these maps have been computed. Given these uncertainties, it was chosen in this work to manufacture and employ three blades that are allowed to pitch around an axis for which $x_P/c = -1, y_P/c = 0$, in order to take advantage of the relative lack of sensitivity around this location.

4. Experimental results

The model-scale tidal turbine was been tested under different operating conditions, as summarised in Table 3. A first set of measurements was carried out by keeping the freestream speed u_∞ constant and equal to $0.5\,\mathrm{m\,s^{-1}}$, while the turbine angular velocity was changed to obtain tip-speed ratios in the range of 3 to 10, as shown in the top part of Table 3. Afterwards, the turbine angular velocity ω was kept constant at $51.3\,\mathrm{rev\,min^{-1}}$, which resulted in $\lambda = 6.45$ at $u_\infty = 0.5\,\mathrm{m\,s^{-1}}$, and the freestream speed was varied in the range of $0.4\,\mathrm{m\,s^{-1}}$ to $0.7\,\mathrm{m\,s^{-1}}$, with the tip-speed ratio changing as shown in the bottom part of Table 3.

This test matrix was repeated for four different configurations. In the first one, the turbine was not yawed with respect to the incoming flow, and the blades were prevented from pitching by fastening the pitch retention and limiting screw on the pitching mechanism chassis; under this configuration, the turbine acts as a canonical speed-controlled, fixed-pitch bladed machine. In the second configuration, the turbine yaw is still kept to zero, but the blades are allowed to pitch: this is obtained by loosening the retention screw, such that each blade is allowed to pitch independently from the fixed-pitch reference as described in Section 2.2. For the second configuration, each spring

Table 3
Test matrix carried out during the campaign.

u_∞ [$\mathrm{m\,s^{-1}}$]	ω [$\mathrm{rev\,min^{-1}}$]	λ
0.4	51.3	8.06
0.5	51.3	6.45
0.6	51.3	5.38
0.7	51.3	4.61
0.5	23.9	3
0.5	31.8	4
0.5	39.8	5
0.5	47.8	6
0.5	51.3	6.45
0.5	55.7	7
0.5	63.7	8
0.5	71.6	9
0.5	79.6	10

was preloaded by an angle $\beta_{\mathrm{pre}} = 447.5°$. The conditions of the third and fourth configuration were the same as those of the first two, but with a yaw angle of 15° between the direction of the freestream speed and the turbine axis. The performance of the turbine will first be presented for the test cases without yaw in Section 4.1, and a comparison to the predictions obtained by the reduced-order code presented in Section 3 will be carried out. The performance of the pitching turbine in yawed conditions is then reported in Section 4.2.

4.1. Non-yawed conditions

The first dataset shown in this section is the thrust and power generated by the turbine with varying freestream velocity. The performance of the turbine at $u_\infty = 0.5\,\mathrm{m\,s^{-1}}$ fitted with passively pitching blades is taken as reference to normalise the thrust and power values from both turbines: this defines T_{ref} and P_{ref} as the values of thrust and power respectively attained by the turbine fitted with pitching blades.

Fig. 8 shows the thrust and power generated by the turbine when fitted with fixed-pitch blades and with passively pitching blades; in addition, the performance predictions for the passively pitching blades obtained using the BEMT code described in Section 3 are shown (see Fig. 5 for the BEMT results for the fixed pitch turbine). One can readily observe that at u_{ref} the thrust and power of the turbine equipped

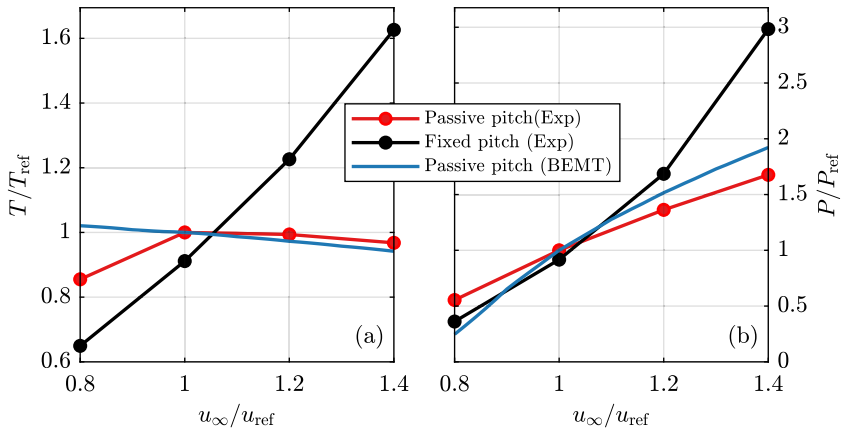

Fig. 8. Thrust (a) and power (b) generated by the model-scale tidal turbine when subject to an inflow having different values of u_∞ in non-yawed conditions. Data for fixed and pitching blades, and synthetic data from the BEMT code described in Section 3.

with fixed-pitch blades and passively pitching blades do not match: this difference is likely due to an erroneous estimation of the preload on the spring used to constrain the motion of the blades. Setting the wrong preload will have resulted in a non-zero pitch of the blades at $u_\infty = u_{\mathrm{ref}}$ and therefore in a slight change in performance for the passive pitch turbine. This might be due to uncertainty in the spring elastic constant, which has only been estimated with an engineering formula. Nonetheless, the observations that can be gathered from these results are not affected, as the spring preload β_{pre} was not changed during the course of the tests.

From the trends of thrust with freestream speed reported in Fig. 8(a), it is evident that for the passive pitch turbine, the thrust is minimally affected by the actual freestream speed for $u_\infty > u_{\mathrm{ref}}$, with the total thrust generated by the turbine being slightly reduced by an increase in the current velocity. In particular, for a $u_\infty/u_{\mathrm{ref}} = 1.4$, this turbine generates a $T/T_{\mathrm{ref}} = 0.97$, or an essentially constant value when compared to the more than 60% increase seen for the fixed-pitch bladed turbine operating at the same freestream speed. For freestream speeds lower than the reference one, instead, it can be seen that thrust generated by the passively pitching blade is larger than that of the equivalent fixed-pitch blade, although the quasi-linear relationship that held for $u_\infty > u_{\mathrm{ref}}$ does not hold true; in fact, the thrust generated by the turbine is at its lowest value. This shows that a turbine equipped with passively pitching blades can intrinsically limit the amount of thrust transferred to the turbine structure without any active control, as the maximum value of thrust is the one attained at $u_\infty = u_{\mathrm{ref}}$ and an increase or decrease in freestream speed results in a reduction in rotor thrust. The power that is generated by the turbine in the same conditions is plotted in Fig. 8(b): from this, it is evident that the power generated by the turbine still follows an increasing trend with freestream speed u_∞; however, the slope of this trend is smaller than that of its fixed-pitch bladed counterpart, and the generated power is therefore less sensitive to the inflow conditions for a turbine equipped with passively pitching blades, as predicted by the maps in Fig. 7(b).

The thrust and torque predicted by the BEMT code are included in Fig. 8 as blue lines. In both the case of thrust and of power, the predictions of the reduced-order code match the experimental results well: this is particularly the case for the turbine thrust at freestream speeds larger than u_{ref}, with a maximum difference of 2.6% at 1.4 u_{ref}, while a slight overestimation of the power generated by the turbine is obtained for the same conditions, with a maximum difference of 13% at 1.4 u_{ref}. For velocities lower than u_{ref} the predictions are less accurate: for example, the low-order code approach cannot accurately capture the departure from the linear trend of $T(u_\infty)$ at low velocities. Here, the maximum difference in thrust is 16%, while the difference in power is 55% at $u_\infty = 0.8u_{\mathrm{ref}}$. This discrepancy is unlikely to be due to friction from the bearings securing the pitching axis in place, as was the case in Gambuzza et al. [41]. In fact, we estimated the mechanical damping from dry tests of the oscillating system to be negligible compared to the hydrodynamic damping. Instead, experimental data is affected by bias and random errors, including, but not limited to, instrument calibration, estimate of the mean velocity due to the non-uniform and non-constant velocity field through the rotor swept area, fluctuations in the turbine angular velocity, blade misalignment, inexact linearity of the spring, etc.

Fig. 9 shows the values of thrust and power coefficient generated by the turbine as the tip-speed ratio λ is changed while keeping u_∞ constant and equal to its reference value. It can be seen that allowing the blades to passively pitch changes the trend of the thrust coefficient drastically: for instance, the maximum value of C_T is attained at $\lambda = 7$ for passively pitching blades, while the thrust generated by its fixed-pitch bladed counterpart plateaus at high values of λ. Some more important observations can be drawn from the trend of the power coefficient C_P with λ. Firstly, one can observe that, apart from a limited range of tip-speed ratios between 5 and 7, the power coefficient of the turbine is less than that of its equivalent fixed-pitch bladed counterpart, and outside this range the power coefficient curve is more sensitive to λ than a canonical turbine. This suggests that a passively pitching turbine blade needs to be carefully designed to ensure that it operates in the narrower range of λ for which a smaller sensitivity to the actual tip-speed ratio is achieved. Fig. 9 also shows the thrust and power coefficients predicted by the reduced-order code informed by BEMT. The maximum difference between the experimental results and those predicted by BEMT is about 9% in thrust and nearly 7% in power at $\lambda = 6$.

As an additional remark, one can observe that for the passively pitching blades, C_P tends to negative values as the tip-speed ratio decreases. This suggests that particular care can be given to the design of the pitching mechanism to ensure that, at low speeds, down to and including $u_\infty = \omega = 0$, the turbine generates positive power (and therefore torque) and can self-start. This negative torque generation is due to the constant balancing moment exerted by the spring: as the tip-speed ratio decreases, the spring pitches the blade progressively to higher negative values of β, as shown in Fig. 10(a). It is noted, however, that a turbine does not need to self-start, as it can be started by providing power to the generator, using it as a motor until the angular velocity is sufficient to invert the torque. If one wants to design a self-starting turbine, then a mechanical limiter to the minimum pitch can be adopted, such that the pitch angle is always sufficient to ensure self-start. For example, an end stop can be adopted to ensure that the minimum pitch angle is the design pitch at power rated, such that the blades keep the same pitch angle at any flow velocity below rated speed and pitch to feather only above rated speed.

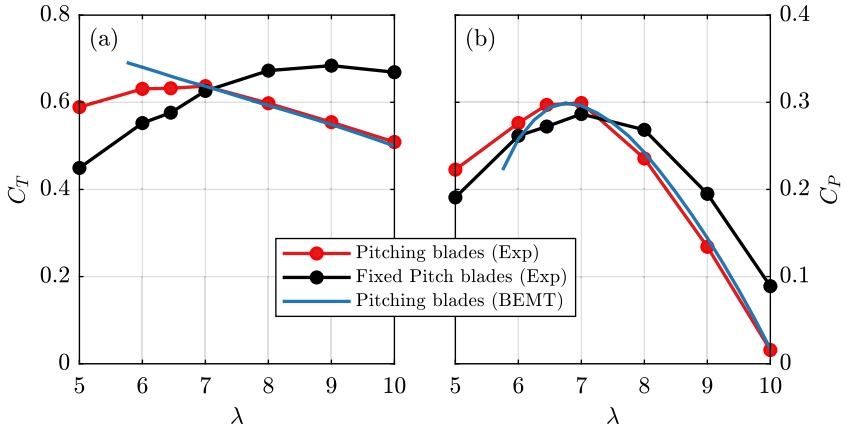

Fig. 9. Thrust (a) and power (b) coefficients generated by the turbine when changing the tip-speed ratio in non-yawed conditions. Experimental data for fixed and pitching blades, and numerical data from the BEMT code described in Section 3.

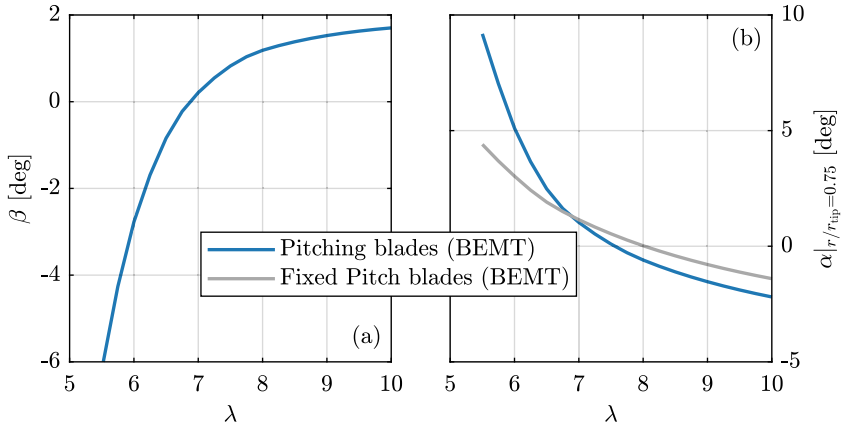

Fig. 10. Blade section pitch (a) and angle of attack (b) at a section at $r/r_{tip} = 0.75$ of the blade as predicted by the low-order code as a function of the tip-speed ratio, for the pitching blade and the fixed-pitch blade.

In the present experiments, at the limiting condition $u_\infty = \omega = 0$, the blade pitches under the effect of the spring alone and the rotation is only constrained by the pitch limiting screw (part I on Fig. 2). Under this configuration, the blade pitch is, therefore, the minimum possible ($-25°$). To ensure the turbine generates torque at low inflow velocities and $\omega = 0$, one shall limit the minimum value of pitch the blades can attain. This can be achieved by a straightforward modification to the pitch limiting system: for the turbine discussed in this paper, the length of the slot in which the limiting screw moves can be changed in the manufacturing step to ensure a minimum value of β that guarantees positive torque at zero ω.

As a result of the changes in pitch, the angle of attack along the blade increases more rapidly for a pitching blade than it does for a fixed-pitch-bladed turbine with decreasing u_∞ and with decreasing ω. Therefore, a turbine equipped with pitching blades may enter stall at higher values of λ, as shown briefly in Fig. 10(b).

4.2. Yawed conditions

This section reports the thrust and power generated under yawed inflow conditions ($\gamma = 15°$) for both fixed and passively pitching blades. Again, the performance of the case with no yaw and pitching blades is used as a reference (i.e., the values of u_{ref}, T_{ref} and P_{ref} are not changed from those of Section 4.1). The spring preload is also unchanged from the previous section.

The effect of yawed inflow is to reduce the average speed seen at the rotor plane by $\cos\gamma$, and to introduce a once-per-revolution variation in the angle of attack on the blade sections. In fact, for a positive yaw angle, and a positive angular velocity about the streamwise axis, the yaw acts to increase the angle of attack when the blade is at the top of its rotation, and reduce it when the blade reaches its lowest position. When the blade is horizontal, the yaw produces a spanwise flow but does not affect the angle of attack.

Fig. 11 shows the thrust and power generated by the turbine with fixed-pitch blades and by the one with passively pitching blades operating under yaw, along with the performance figures previously reported in Fig. 8 for the pitching and fixed blades under no yaw. Immediately, it can be seen that the performance of the turbine equipped with the passive pitching system is only minimally affected by the non-zero yaw conditions: this is evident both in the thrust and the power measurements, both for different u_∞ (Fig. 11) and for differet λ values (Fig. 12). In comparison, the thrust and power generated by the turbine equipped with fixed-pitch blades have decreased by a constant factor of $\cos^2(15°)$ and $\cos^3(15°)$ respectively (Fig. 11). This suggests that the passive pitch is able to counteract the angle of attack perturbation due to the yawed inflow. Some minor differences between the two pitching test cases, however, are present: for instance, it can be seen that the thrust generated by the turbine slightly increases with increasing u_∞ for the case where yaw is present, while this is not observed for the $\gamma = 0$ case; however, this increase is minor, amounting only to 3% of T_{ref} at $u_\infty/u_{ref} = 1.4$. Instead, with passive pitch, differences between the power harvested at different yaw angles are negligible at every λ. The results shown in this section suggest that the passive pitch system is capable of mitigating flow fluctuations at frequencies at least up to and including the turbine rotational speed. Note that, for the yawed test cases, no comparison with BEMT predictions is offered as

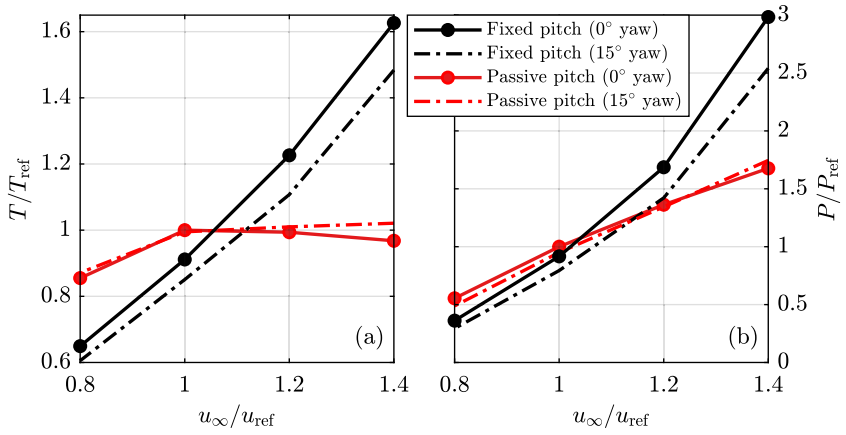

Fig. 11. Thrust (a) and power (b) generated by the turbine when subject to an inflow having different values of u_∞ in different yaw conditions.

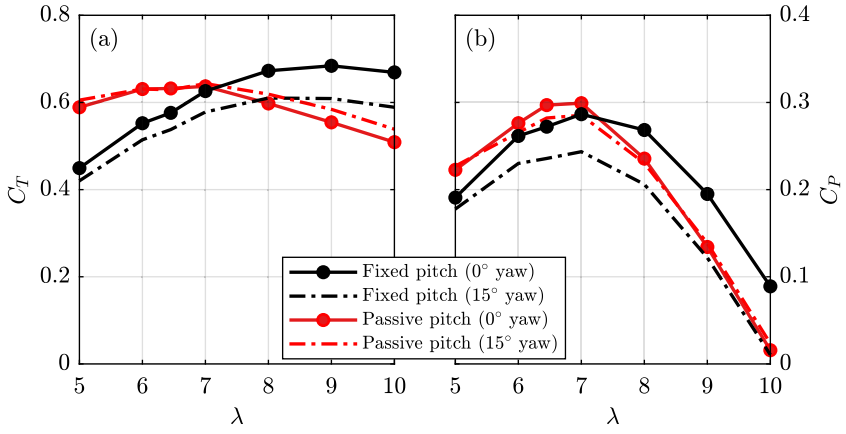

Fig. 12. Thrust (a) and power (b) coefficients generated by the turbine when changing the tip-speed ratio in different yaw conditions.

the theoretical background presented in Section 3 does not account for the presence of yaw.

4.3. Performance during a tidal period

Having observed the performance of the passive pitch system, and in particular the trends of power and thrust as functions of the freestream speed u_∞, we can estimate the loading and performance of a turbine equipped with passively pitching blades in a realistic inflow. To gauge how this passive control system compares to the current state-of-the-art in terms of speed- and pitch-controlled turbines, we use the BEMT data previously shown to simulate two hypothetical turbines harvesting power from an idealised, sinusoidal flow representative of the flow seen by a tidal turbine during a tidal cycle. The sinusoidal flow follows the time history

$$\frac{u_\infty(t)}{u_{\text{ref}}} = \frac{u_{\text{rated}}}{u_\infty} - 0.2\cos\left(2\pi\frac{t}{\tau}\right) \quad t \in [0;\tau], \tag{20}$$

where τ is the tidal period, u_{rated} is chosen to be $1.2\,u_\infty$ and the amplitude is chosen so that $u_\infty/u_{\text{ref}} \in [1; 1.4]$ to match the available experimental data from the tidal turbine equipped with pitching blades.

The state-of-the-art is represented by a speed- and pitch-controlled turbine, whose controller aims to keep the harvested power below a maximum value, P_{rated}, which is itself computed as the maximum power the turbine can harvest when $u_\infty = u_{\text{rated}}$. For freestream speeds below u_{rated}, the controller sets both the tip-speed ratio λ and the blade pitch β to maximise the generated power; for higher speeds, the controller keeps $P = P_{\text{rated}}$ by mandating a constant angular velocity ω_{rated} and increasing the blade pitch. The angular velocity ω_{rated} is the value of ω at which the turbine operates for $u_\infty \to u_{\text{rated}}$.

The passively pitching turbine is modelled as a speed-controlled turbine in which the pitch angle β is not mandated by the controller, but inferred for each operating condition from Eq. (19). As with the state-of-the-art device, the controller of the passive pitch turbine maximises the power generated for $u_\infty < u_{\text{rated}}$, and keeps $P = P_{\text{rated}}$ for $u_\infty > u_{\text{rated}}$ by increasing the pitch angle; as direct control of the pitch is unavailable, the increase in β is obtained indirectly by increasing the turbine angular velocity, and therefore by increasing λ. The spring preload is set so the blade has a pitch angle β of 0° when $u_\infty = u_{\text{rated}}$ and $\lambda = \lambda_{\text{rated}}$.

The time-histories of the angular velocity and the generated loads for the two devices are shown in Fig. 13. It can be seen that the turbine equipped with passively pitching blades is able, by means of only controlling the turbine angular velocity, to track the power generated by the actively controlled turbine, as shown in Fig. 13(c): in fact, the two time-histories of generated power match well over the whole tidal period, except when $u \approx u_{\text{ref}}$, where a slight loss in power is observed. Conversely, the thrust time-histories of the two devices are visibly different, as seen in Fig. 13(d): the passively pitching turbine manages to generate both a lower maximum value of thrust and a lower standard deviation of it over the whole tidal period. This reduced thrust loading comes at a cost of a more complicated angular velocity controller: as can be seen in Fig. 13(b), the rotor speed is not constant for $u_\infty > u_{\text{rated}}$: as u_∞ increases, ω must increase in order to increase the blade pitch and ultimately keep the power constant.

5. Discussion and conclusions

This paper has shown the effectiveness of passive pitch in reducing fluctuations in torque and thrust on a tidal turbine due to

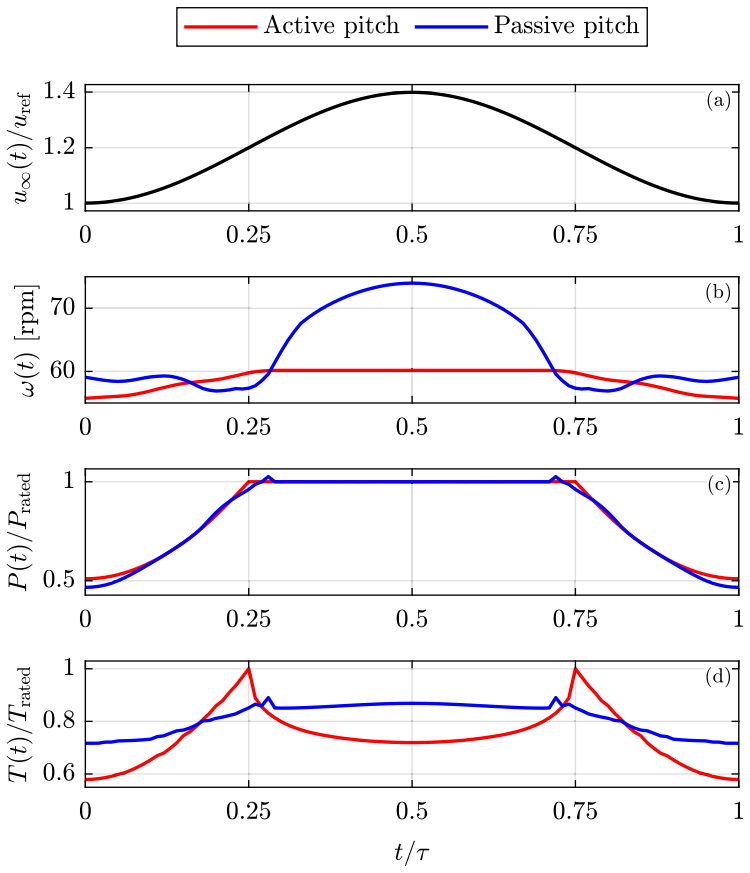

Fig. 13. Time-history of the freestream speed (a) during a simulated tidal cycle, and timeseries of the angular velocity ω (b), generated power (c) and thrust (d) for a turbine equipped with a fully active controller and one with passive pitch and active speed controller.

quasi-steady changes in inflow and operating conditions. Furthermore, passive pitch has been shown to mitigate the power reduction due to yaw misalignment with the free stream.

The main conclusion of this paper is that the passive pitch system could entirely replace the active pitch system while achieving the same energy yield over the tidal period and a lower thrust force on the support structures. This would allow lighter and cheaper structures, reducing CAPEX and OPEX, while simplifying the turbine design and control, increasing reliability. Furthermore, these results show that the passive pitch systems decreases the sensitivity to the yaw and thus alleviates the requirement of the yaw control system. Finally, it is also noted that for seabed-mounted turbines, controlling the active pitch system requires at least three cores of the cable which connects the turbine to the shore, and the reliability of each core and connector is a critical technical challenge for the sector. Overall, these results directly contribute to addressing three of the ten areas that have the greatest potential for reducing the LCOE [28]: increasing reliability and decreasing costs of pitch control systems, increasing lifetime performance, and increasing turbine diameter. These together could contribute to a 35% LCOE reduction [28], resulting in a step increase in tidal energy competitiveness and accelerating the transition to a sustainable and resilient net zero future.

A low-order code based on Blade Element Momentum Theory was used to identify the optimal pitching axis location to limit the variations in the thrust and torque transferred to the turbine structure in the presence of changes in freestream speed and direction. The optimal pitching axis was found to be parallel to the blade span, upstream in the chordwise direction and upstream in the chordnormal direction. Its exact position can be chosen to minimise either the thrust or the torque (and thus power) variations due to changes in the freestream speed or direction. For the specific foil sections of the blades chosen for this study, a pitching axis through a point about one chord upstream of the quarter-chord point in the chordwise direction with no chordnormal displacement allows a substantial reduction in both thrust and torque variations. Furthermore, the sensitivity to the exact position of the pitching axis on the thrust and torque unsteady mitigation is marginal.

Experimental tests were performed on a model-scale turbine in a recirculating open water channel. The freestream speed, turbine angular velocity and turbine yaw angle with the free stream were all varied systematically. The predictions of the reduced-order model matched well with the experimental results, both for the turbine with fixed pitch, and those with passive pitch. The agreement was less good at low u_∞ – attributed to high friction around the pitch mechanism shaft – and at low λ, where substantial flow separation is likely.

The thrust generated by the turbine equipped with passively pitching blades was insensitive to changes in the freestream speed: an increase of 40% in the current speed induced a reduction in the generated thrust of 3%. The effect of u_∞ changes on the power generated by the passive pitch turbine was more pronounced, although the power curve was seen to be less sensitive to variations in freestream speed than that of a turbine equipped with fixed-pitch blades. It was also observed that the maximum pitching angle allowed by the passive system can be limited to ensure good performance at low angular velocity and enable self starting.

The turbine was also tested with yawed inflow, which was set to 15° for this study. Without changing the spring preload and therefore the settings of the pitching apparatus, the performance of the turbine equipped with pitching blades under yaw matches the performance of the same turbine under no yaw: this shows that a turbine equipped with this passive system is insensitive to moderate misalignment between the turbine axis and the freestream.

Finally, the experimental results were used to model the operation of a turbine through an entire tidal cycle. Because the blades pitch to feather as the angular velocity increases, it is possible to control the power harvested indirectly through the angular velocity. Specifically, a turbine equipped with a passive pitch system can provide the same power output as a turbine with active pitch, although a marginal increase in the angular velocity is required in order to keep the power constant. Furthermore, the maximum thrust experienced by a turbine with active pitch is substantially lower for a turbine with passive pitch.

Overall, this research demonstrates that a passive pitch control is a viable alternative to active pitch control for tidal turbines. It allows the same energy yield over a tidal cycle and comparable control on the power output than an active pitch control. Passive pitch also has the advantage of allowing a lower maximum thrust over the tidal cycle, lower thrust and power fluctuations, and lower sensitivity to yaw misalignment.

CRediT authorship contribution statement

Stefano Gambuzza: Writing – original draft, Visualization, Validation, Software, Methodology, Investigation, Formal analysis, Data curation, Conceptualization. **Puja Sunil:** Writing – review & editing, Writing – original draft, Visualization. **Mario Felli:** Writing – review & editing, Resources. **Anna M. Young:** Writing – review & editing, Supervision, Methodology, Investigation, Funding acquisition, Conceptualization. **Riccardo Broglia:** Writing – review & editing, Supervision, Resources. **Edward D. McCarthy:** Writing – review & editing, Supervision, Funding acquisition. **Ignazio Maria Viola:** Writing – review & editing, Writing – original draft, Supervision, Resources, Project administration, Funding acquisition, Conceptualization.

Declaration of competing interest

The authors declare the following financial interests/personal relationships which may be considered as potential competing interests: Ignazio Maria Viola reports financial support was provided by Engineering and Physical Sciences Research Council. Edward McCarthy reports financial support was provided by Engineering and Physical Sciences Research Council. Anna Young reports financial support was provided by Engineering and Physical Sciences Research Council. Stefano Gambuzza reports financial support was provided by Engineering and Physical Sciences Research Council. Puja Sunil reports financial support was provided by Engineering and Physical Sciences Research Council. Ignazio Maria Viola has patent #PCT/GB2024/050216 pending to University of Edinburgh. Edward McCarthy has patent #PCT/GB2024/050216 pending to University of Edinburgh. Stefano Gambuzza has patent #PCT/GB2024/050216 pending to University of Edinburgh. If there are other authors, they declare that they have no known competing financial interests or personal relationships that could have appeared to influence the work reported in this paper.

Acknowledgements

This work was supported by the UK Engineering and Physical Sciences Research Council through the grant ‘Morphing-Blades: New-Concept Turbine Blades for Unsteady Load Mitigation’ [EP/V0094 43/1].

References

[1] O.E. Systems, Ocean energy and net zero: An international roadmap to develop 300GW of ocean energy by 2050, 2023, https://www.ocean-energy-systems.org/publications/oes-documents/market-policy-/document/ocean-energy-and-net-zero-an-international-roadmap-to-develop-300gw-of-ocean-energy-by-2050/, November 23, 2024.

[2] S.P. Neill, K.A. Haas, J. Thiébot, Z. Yang, A review of tidal energy—Resource, feedbacks, and environmental interactions, J. Renew. Sustain. Energy 13 (6) (2021) http://dx.doi.org/10.1063/5.0069452.

[3] T.A. Adcock, S. Draper, G.T. Houlsby, A.G. Borthwick, S. ogluSena, The available power from tidal stream turbines in the Pentland Firth, Proc. R. Soc. A: Math. Phys. Eng. Sci. 469 (2157) (2013) 20130072, http://dx.doi.org/10.1098/rspa.2013.0072.

[4] E.A. Bossanyi, The design of closed loop controllers for wind turbines, Wind Energy: Int. J. Prog. Appl. Wind Power Convers. Technol. 3 (3) (2000) 149–163, http://dx.doi.org/10.1002/we.34.

[5] L. Chen, W.-H. Lam, A review of survivability and remedial actions of tidal current turbines, Renew. Sustain. Energy Rev. 43 (2015) 891–900, http://dx.doi.org/10.1016/j.rser.2014.11.071.

[6] T.A. Adcock, S. Draper, R.H. Willden, C.R. Vogel, The fluid mechanics of tidal stream energy conversion, Annu. Rev. Fluid Mech. 53 (2021) 287–310, http://dx.doi.org/10.1146/annurev-fluid-010719-060207.

[7] G.T. Scarlett, B. Sellar, T. Van Den Bremer, I.M. Viola, Unsteady hydrodynamics of a full-scale tidal turbine operating in large wave conditions, Renew. Energy 143 (2019) 199–213, http://dx.doi.org/10.1016/j.renene.2019.04.123.

[8] G.T. Scarlett, I.M. Viola, Unsteady hydrodynamics of tidal turbine blades, Renew. Energy 146 (2020) 843–855, http://dx.doi.org/10.1016/j.renene.2019.06.153.

[9] C. Greenwood, A. Vogler, V. Venugopal, On the variation of turbulence in a high-velocity tidal channel, Energies 12 (4) (2019) 672, http://dx.doi.org/10.3390/en12040672.

[10] P. Ouro, T. Nishino, Performance and wake characteristics of tidal turbines in an infinitely large array, J. Fluid Mech. 925 (2021) A30, http://dx.doi.org/10.1017/jfm.2021.692.

[11] J. McNaughton, B. Cao, A. Nambiar, T. Davey, C.R. Vogel, R.H. Willden, Constructive interference effects for tidal turbine arrays, J. Fluid Mech. 943 (2022) A38, http://dx.doi.org/10.1017/jfm.2022.454.

[12] J. Schluntz, R.H. Willden, The effect of blockage on tidal turbine rotor design and performance, Renew. Energy 81 (2015) 432–441, http://dx.doi.org/10.1016/j.renene.2015.02.050.

[13] H. Ross, B. Polagye, An experimental assessment of analytical blockage corrections for turbines, Renew. Energy 152 (2020) 1328–1341, http://dx.doi.org/10.1016/j.renene.2020.01.135.

[14] I.M. Viola, Z. Gao, J. Smith, Use of streamnormal forces within an array of tidal power harvesters, Plos One 17 (7) (2022) e0270578, http://dx.doi.org/10.1371/journal.pone.0270578.

[15] I. Milne, A. Day, R. Sharma, R. Flay, Blade loading on tidal turbines for uniform unsteady flow, Renew. Energy 77 (2015) 338–350, http://dx.doi.org/10.1016/j.renene.2014.12.028.

[16] I. Milne, A. Day, R. Sharma, R. Flay, The characterisation of the hydrodynamic loads on tidal turbines due to turbulence, Renew. Sustain. Energy Rev. 56 (2016) 851–864, http://dx.doi.org/10.1016/j.rser.2015.11.095.

[17] P.W. Galloway, L.E. Myers, A.S. Bahaj, Quantifying wave and yaw effects on a scale tidal stream turbine, Renew. Energy 63 (2014) 297–307, http://dx.doi.org/10.1016/j.renene.2013.09.030.

[18] A. El Yaakoubi, A. Bouzem, R. El Alami, N. Chaibi, O. Bendaou, Wind turbines dynamics loads alleviation: Overview of the active controls and the corresponding strategies, Ocean Eng. 278 (2023) 114070, http://dx.doi.org/10.1016/j.oceaneng.2023.114070.

[19] M.A. Lackner, G. van Kuik, A comparison of smart rotor control approaches using trailing edge flaps and individual pitch control, Wind Energy: Int. J. Prog. Appl. Wind Power Convers. Technol. 13 (2–3) (2010) 117–134, http://dx.doi.org/10.1002/we.353.

[20] T.K. Barlas, W. Van Wingerden, A. Hulskamp, G.M. van Kuik, H.N. Bersee, Smart dynamic rotor control using active flaps on a small-scale wind turbine: aeroelastic modeling and comparison with wind tunnel measurements, Wind Energy 16 (8) (2013) 1287–1301, http://dx.doi.org/10.1002/we.1560.

[21] J. Smit, L.O. Bernhammer, S.T. Navalkar, L. Bergami, M. Gaunaa, Sizing and control of trailing edge flaps on a smart rotor for maximum power generation in low fatigue wind regimes, Wind Energy 19 (4) (2016) 607–624, http://dx.doi.org/10.1002/we.1853.

[22] H. Wang, X. Jiang, Y. Chao, Q. Li, M. Li, W. Zheng, T. Chen, Effects of leading edge slat on flow separation and aerodynamic performance of wind turbine, Energy 182 (2019) 988–998, http://dx.doi.org/10.1016/j.energy.2019.06.096.

[23] A. Zaki, M. Abdelrahman, S.S. Ayad, O. Abdellatif, Effects of leading edge slat on the aerodynamic performance of low Reynolds number horizontal axis wind turbine, Energy 239 (2022) 122338, http://dx.doi.org/10.1016/j.energy.2021.122338.

[24] S.J. Johnson, J.P. Baker, C. Van Dam, D. Berg, An overview of active load control techniques for wind turbines with an emphasis on microtabs, Wind Energy: Int. J. Prog. Appl. Wind Power Convers. Technol. 13 (2–3) (2010) 239–253, http://dx.doi.org/10.1002/we.356.

[25] A.M. Cooperman, R. Chow, C. Van Dam, Active load control of a wind turbine airfoil using microtabs, J. Aircr. 50 (4) (2013) 1150–1158, http://dx.doi.org/10.2514/1.C032083.

[26] L.O. Bernhammer, G.A. van Kuik, R. De Breuker, Fatigue and extreme load reduction of wind turbine components using smart rotors, J. Wind Eng. Ind. Aerodyn. 154 (2016) 84–95, http://dx.doi.org/10.1016/j.jweia.2016.04.001.

[27] A.M. Young, J.R. Farman, R.J. Miller, Load alleviation technology for extending life in tidal turbines, in: Progress in Renewable Energies Offshore: Proceedings of the 2nd International Conference on Renewable Energies, 2016, RENEW2016, Taylor & Francis Books Ltd, 2016, pp. 521–529, http://dx.doi.org/10.17863/CAM.99753.

[28] C.R. Energy, Tidalstreamtechnologyroadmap, 2024, https://cms.ore.catapult.org.uk/wp-content/uploads/2024/03/ORE-Catapult-Tidal-stream-roadmap-report-2024.pdf, November 23, 2024.

[29] C.L. Bottasso, A. Croce, F. Gualdoni, P. Montinari, Load mitigation for wind turbines by a passive aeroelastic device, J. Wind Eng. Ind. Aerodyn. 148 (2016) 57–69, http://dx.doi.org/10.1016/j.jweia.2015.11.001.

[30] A. Arredondo-Galeana, A.M. Young, A.S. Smyth, I.M. Viola, Unsteady load mitigation through a passive trailing-edge flap, J. Fluids Struct. 106 (2021) 103352, http://dx.doi.org/10.1016/j.jfluidstructs.2021.103352.

[31] U. Cordes, B. Lambie, K. Hufnagel, H. Spiegelberg, G. Kampers, C. Tropea, The Adaptive Camber Concept—A passive approach for gust load alleviation on wind turbines, Wind Energy 21 (9) (2018) 732–744, http://dx.doi.org/10.1002/we.2190.

[32] S. Hoerner, S. Abbaszadeh, O. Cleynen, C. Bonamy, T. Maître, D. Thévenin, Passive flow control mechanisms with bioinspired flexible blades in cross-flow tidal turbines, Exp. Fluids 62 (2021) 1–14, http://dx.doi.org/10.1007/s00348-021-03186-8.

[33] R. Murray, S. Ordonez-Sanchez, K.E. Porter, C.M. Johnstone, D.A. Doman, M.J. Pegg, Towing Tank and Flume Testing of Passively Adaptive Composite Tidal Turbine Blades, Tech. rep., National Renewable Energy Lab.(NREL), Golden, CO (United States), 2017, URL https://www.nrel.gov/docs/fy17osti/68107.pdf.

[34] K. Van Ness, A. Aliseda, B. Polagye, Experimental comparison of passive adaptive blade pitch control strategies for an axial-flow current turbine, J. Ocean Eng. Mar. Energy 10 (1) (2024) 105–123, http://dx.doi.org/10.1007/s40722-023-00302-0.

[35] F.Z. de Arcos, C.R. Vogel, R.H. Willden, Hydrodynamic independence and passive control application of twist and flapwise deformations of tidal turbine blades, J. Fluids Struct. 118 (2023) 103827, http://dx.doi.org/10.1016/j.jfluidstructs.2022.103827.

[36] Y. Liu, R. Broglia, A.M. Young, E.D. McCarthy, I.M. Viola, Unsteady load mitigation through passive pitch, J. Fluids Struct. 131 (2024) 104216, http://dx.doi.org/10.1016/j.jfluidstructs.2024.104216.

[37] S. Ōtomo, S. Gambuzza, Y. Liu, A.M. Young, R. Broglia, E.D. McCarthy, I.M. Viola, A general framework for the design of efficient passive pitch systems, Phys. Fluids 36 (6) (2024) URL https://doi.org/10.1063/5.0212626.

[38] I.M. Viola, G. Pisetta, W. Dai, A. Arredondo-Galeana, A. Young, A. Smyth, Morphing blades: Theory and proof of principles, Int. Mar. Energy J. 5 (2) (2022) 183–193, http://dx.doi.org/10.36688/imej.5.183-193, URL https://marineenergyjournal.org/imej/article/view/126.

[39] G. Pisetta, R. Le Mestre, I.M. Viola, Morphing blades for tidal turbines: A theoretical study, Renew. Energy 183 (2022) 802–819, http://dx.doi.org/10.1016/j.renene.2021.10.085.

[40] W. Dai, R. Broglia, I.M. Viola, Mitigation of rotor thrust fluctuations through passive pitch, J. Fluids Struct. 112 (2022) 103599, http://dx.doi.org/10.1016/j.jfluidstructs.2022.103599.

[41] S. Gambuzza, G. Pisetta, T. Davey, J. Steynor, I.M. Viola, Model-scale experiments of passive pitch control for tidal turbines, Renew. Energy 205 (2023) 10–29, http://dx.doi.org/10.1016/j.renene.2023.01.051.

[42] A. Pecoraro, F. Di Felice, M. Felli, F. Salvatore, M. Viviani, An improved wake description by higher order velocity statistical moments for single screw vessel, Ocean Eng. 108 (2015) 181–190, http://dx.doi.org/10.1016/j.oceaneng.2015.07.038.

[43] L. Wang, J.E. Martin, M. Felli, P.M. Carrica, Experiments and CFD for the propeller wake of a generic submarine operating near the surface, Ocean Eng. 206 (2020) 107304, http://dx.doi.org/10.1016/j.oceaneng.2020.107304.

[44] G. Calcagno, F. Di Felice, M. Felli, F. Pereira, A stereo-PIV investigation of a propeller's wake behind a ship model in a large free-surface tunnel, Mar. Technol. Soc. J. 39 (2) (2005) 94–102, http://dx.doi.org/10.4031/002533205787444051.

[45] M. Tanaka, G. Girard, R. Davis, A. Peuto, N. Bignell, Recommended table for the density of water between 0 C and 40 C based on recent experimental reports, Metrologia 38 (4) (2001) 301–309, http://dx.doi.org/10.1088/0026-1394/38/4/3.

[46] L. Korson, W. Drost-Hansen, F.J. Millero, Viscosity of water at various temperatures, J. Phys. Chem. 73 (1) (1969) 34–39, http://dx.doi.org/10.1021/j100721a006.

[47] S.A. Ning, A simple solution method for the blade element momentum equations with guaranteed convergence, Wind Energy 17 (9) (2014) 1327–1345, http://dx.doi.org/10.1002/we.1636.

[48] H. GIanert, Airplane Propellers, Springer, 1935, http://dx.doi.org/10.1007/978-3-642-91487-4_3.

[49] M.L. Buhl Jr., New Empirical Relationship Between Thrust Coefficient and Induction Factor for the Turbulent Windmill State, Tech. rep., National Renewable Energy Lab.(NREL), Golden, CO (United States), 2005, http://dx.doi.org/10.2172/15016819.

[50] M. Drela, XFOIL: An analysis and design system for low Reynolds number airfoils, in: Low Reynolds Number Aerodynamics, Springer, Berlin, Heidelberg, 1989, pp. 1–12, http://dx.doi.org/10.1007/978-3-642-84010-4_1.